Energy 262 (2023) 125350

Contents lists available at ScienceDirect

Energy

journal homepage: www.elsevier.com/locate/energy

Fast online reinforcement learning control of small lift-driven vertical axis wind turbines with an active programmable four bar linkage mechanism

He Shen [a,*], Alexis Ruiz [a], Ni Li [b,**]

[a] Department of Mechanical Engineering, California State University, Los Angeles, CA, 90032, USA
[b] Department of Aeronautics, Northwestern Polytechnical University, Xian, Shaanxi, 710072, China

ARTICLE INFO

Keywords:
Vertical axis wind turbine
Pitch control
Four bar linkage mechanism
Reinforcement learning
Transient response

ABSTRACT

Maintaining high power generation for small lift-driven vertical axis wind turbines in a changing wind environment has not been well studied yet, due to the challenges inherited from the unpredictable turbulent flow-blade interaction and complex blade interferences. Herein, a fast online reinforcement learning pitch control using an active programmable four bar linkage mechanism is proposed, making it possible for turbines to quickly adapt to wind changes and maintain high power output in operation. We formulate the pitching mechanism using a drag-link configuration with a variable frame link length into an optimization problem and further solve it by the interior point algorithm under a wide range of tip speed ratios. Then, a parameter explorative policy gradient reinforcement learning method is designed for the turbine to adaptively tune the frame link length. Since the design significantly reduces the number of parameters needed to depict a whole pitch trajectory, the proposed online learning process can converge quickly, making it capable of handling complex wind conditions in an urban environment. The transient behavior overlooked in much of the literature is also studied. Comparisons to two benchmarks have demonstrated that our proposed system has a superior performance.

1. Introduction and background

Wind turbines are devices to harvest wind energy, which is one of the fastest-growing renewable technologies. According to a report from the National Geographic Society on wind energy, the global demand for wind power is very strong with an expected compound annual growth rate of 5.2% from 2020 to 2027. The increasing need for wind energy makes the study of improving the energy conversion efficiency of wind turbines a hot research topic.

Wind turbines can be broadly categorized into two types – horizontal axis wind turbines (HAWTs) and vertical axis wind turbines (VAWTs). Most of the installed large wind turbines are still HAWTs as they are more efficient and reliable since their research and development are more well established compared to their counterparts. However, recent studies show that VAWTs have many advantages over HAWTs [1–3]. First, the impression of the low efficiency of VAWTs was mostly predicated on passive turbines without an active pitch control mechanism. Many recent studies have shown that VAWTs with proper designs can achieve higher efficiencies than conventional HAWTs in unfavorable wind conditions, such as gusty wind in urban areas [4,5]. It has also been reported that wind farms with VAWTs can potentially achieve a power density that is an order of magnitude higher than those with HAWTs [6]. Second, VAWTs are simple in design and easy for manufacturing. For example, H-rotors use straight blades since they rotate at the same speed, while HAWTs must have much more complex profile designs to accommodate the effective wind speed difference along the span-wise direction. Third, VAWTs operate omnidirectionally without a need for a yaw control system to redirect the turbine towards the wind. In addition, their vertical rotational axis allows the generator to be installed at the bottom of the tower; thereby, VAWTs require lighter structures to support the wind load and are easier to install, operate, and maintain [4]. Aside from the listed benefits, the prevalent self-starting incapability associated with VAWTs due to low torque generation at lower speeds has been extensively studied. Abdolahifar and Karimian proposed a slotted blade design to increase output torque at low tip speed ratios by reducing flow separation effects [1]. Celik et al. investigated the startup performance of J-shaped airfoils with varying opening ratios to attempt improved self-starting abilities [2]. Introducing pitch controls is another way to improve self-starting capabilities by avoiding stalling at low tip speed ratios and minimizing negative

* Corresponding author. Department of Mechanical Engineering, California State University, Los Angeles, CA, 90032, USA.
** Corresponding author.
E-mail addresses: hshen6@calstatela.edu (H. Shen), lini@nwpu.edu.cn (N. Li).

https://doi.org/10.1016/j.energy.2022.125350
Received 23 April 2022; Received in revised form 29 July 2022; Accepted 30 August 2022
Available online 5 September 2022

torque regions in operation [4,7]. Pitch control is also used to lower load fluctuation, reduce structural vibration, and alleviate dynamic stall [8–10].

Research for VAWTs without pitching control mechanisms is mainly focused on design optimization and operation improvement. Islam et al. studied the geometric features of airfoils for straight bladed VAWTs and found that asymmetric airfoils are advantageous for operations at designated low tip speed ratios [11]. Zhang el al. designed a bionic blade with convex structures at the leading edge to deter flow separation stall for improved performance [12]. Aside from airfoil designs, researchers also explored the impact of the geometry parameters of turbines on their performance. For example, Tian et al. developed a Savonius VAWT with overlapped rotors and studied the influence of the distance between adjacent rotors on their performance [13]. Cuevas-Carvajal et al. presented the influence of the turbine's aspect ratio, number of blades, angle of attack, twist angle, overlap ratio, and number of stages, on the performance of Savonius VAWTs [14]. Peng et al. used metal grids of different materials to simulate varying turbulent conditions. From there, they studied the impact of four variables (i.e., pitch angle, solidity, aspect ratio, and turbulent intensity) on the performance of a VAWT and found that pitch angle had the most impact on performance [15]. Improvements by controlling local wind conditions have also been studied. For example, Chen et al. implemented a deflector under unsteady wind conditions and studied the varying parameters which improved performance. They concluded tip speed ratio was the factor that contributed to increased performance [16]. To facilitate testing of VAWTs, Santamaria et al. designed an active driving system to mimic the wind effect on the turbine for performance characterization under various mean wind speeds, mean tip speed ratios, and fluctuation speeds and frequencies [17].

Depending on the driving force for spinning, VAWTs can be further divided into two types, lift-driven, and drag-driven turbines. Building upon the extensive study of airfoils for aircraft, lift-driven VAWTs can achieve much higher efficiencies than those powered by drag [18–20]. Hence, the increasing global demand for wind energy cannot be fulfilled without continuous improvement in the efficiency of the lift-driven VAWTs. There have been a lot of studies trying to improve the efficiency of lift-driven VAWTs from many perspectives, such as blade and turbine design, flow control, profile modification, blade number, and pitch control [21–23]. Since pitch control can always be used to boost energy efficiency regardless of the design, this paper focuses on improving the performance of lift-driven VAWTs with pitch control mechanisms.

Pitch control can be implemented in either a passive or active manner. The passive pitch control mechanism typically uses the inertial and aerodynamic forces acting on the blade to dynamically adjust the pitch angle of the blades [24]. In the area of active pitch control, the turbine blades can be either controlled individually by motors or collectively with additional mechanisms. Due to the cyclic nature of the motion of all blades with a fixed phase difference, individual control with multiple motors seems cumbersome and requires a significant amount of power to constantly vary pitching angles. Hence, collective active pitch control mechanisms are more popular, and the commonly used mechanisms include 1) synchronized belt wheels driven by a motor [25], 2) eccentric cam with spools [26], 3) four bar linkage mechanism [24,27], and 4) the eccentric disc mechanism [28]. More details on the summary of these different pitch control mechanisms can be found in Ref. [29]. Among all these mechanisms, the four bar linkage mechanism is the most popular due to its simplicity in design and implementation, as well as low energy consumption.

As for the control methods, both the classic PID control and modern model-based control methods are used for pitch control of VAWTs. Hand and Balas designed a PID pitch controller based on two linearized models about two operation points. The controller minimizes the error between the reference and the actual rotation speed of the turbine [30]. The performance is dependent on the choices of points for linearization. Model-based controllers are also designed for pitch control. For example, Camblong developed a digital robust controller by using an average dynamics model for all operating conditions [31]. Moradi and Vossoughi also proposed a robust control to deal with uncertainties and compared the performance of H_∞ and PID controllers [32]. Considering the inevitable parameter uncertainties and unmodeled dynamics inherited from model linearization and manufacturing deficiencies, multiple adaptive control methods are used for pitch control of VAWTs. Sakamoto et al. developed a minimum variance control to compensate for the parameter variations that caused changes in system dynamics [33]. Hatami et al. proposed an adaptive control by combining a least square estimator and a PID controller with adjustable gains to reduce the fatigue load of small VAWTs [34]. To maximize power generation, optimization is also widely used to obtain an ideal pitch trajectory for control. Abdalrahman et al. studied the aerodynamic performance of a 2D VAWT model at a variety of tip speed ratios by using ANSYS Fluent Computational Fluid Dynamics (CFD) and further developed an open-loop pitch angle controller with a multi-layer neural network [35]. Li et al. formulated a relationship between blade pitch and power output by using five parameters. Based on the formulation, optimal blade pitching is found from the genetic algorithm based on CFD simulations [36]. Paraschivoiu et al. formulated the pitch trajectory as an analytical polynomial function of the azimuth angle with unknown coefficients and used the genetic algorithm to optimize these coefficients and further obtained an optimal pitch control policy [37]. In addition, some artificial intelligence methods are used to improve the operation of VAWTs under various wind conditions. Abdalrahman et al. designed a multiple-layer artificial neural network-based controller by using the CFD simulated data and compared it to the performance of a PID controller [35].

However, the aerodynamics of VAWTs are extremely hard to simulate due to the interference effect and turbulent flow caused by the upstream turbine blades over blades downstream. Hence, many simulation-based offline training methods have limitations inherited from the accuracy of the simulation methods used. Moreover, the wind is very hard to predict and can change rapidly, especially in urban wind environments where small VAWTs are used. Almost all wind turbines are designed to operate at an ideal operation point (with a typical tips speed ratio) with the highest energy generation efficiency and their efficiency decreases as the wind speed falls out of a designed preferable zone. To overcome this problem, we proposed a VAWT design with reinforcement learning pitch control with a programmable four bar linkage mechanism. The design of the pitch control mechanism is formulated as an optimization problem and solved by using the interior-point algorithm. The programmable four bar linkage mechanism will constrain the optimization problem within a suboptimal subspace and presents a significant advantage in parameter reduction. It allows online reinforcement learning to converge within a short time of around 30 s, making it suitable for practical applications. The main contributions of this paper are summarized as follows.

1) A programmable four bar linkage mechanism for pitch control of small lift-driven VAWTs is proposed. It significantly reduces the number of parameters needed to describe a complex pitching trajectory and allows us to use only one variable to achieve desired pitch controls.
2) An optimization formulation to design an active programmable four bar linkage mechanism with a length-varying frame link in a drag-link configuration for VAWTs is proposed, making it possible to achieve a quick closed-chain linkage design that can produce pitching trajectories.
3) Based on the programmable four bar linkage mechanism design, an online reinforcement learning control is proposed, which enables the turbine to have the intelligence to adapt to wind changes.
4) The start-up transient performance of the proposed turbine design with reinforcement learning is analyzed and compared to systems

with a constant pitch angle and those with a fixed four bar linkage pitching mechanism.

5) The simulation package that consists of aerodynamics analysis, rotation dynamics, load control, pitch control, and reinforcement learning, can be used for other studies of small VAWTs.

The rest of the paper is organized as follows. In section 2, the preliminaries on load analysis, fluid analysis, and dynamics of VAWTs will be introduced. In section 3, the system design optimization and intelligent reinforcement learning control are presented. In section 4, the results of the system's performance in response to both constant and varying wind conditions, as well as its self-starting performance are provided. Comparisons to other VAWTs in both steady and transient behaviors are provided. In section 5, we discuss the choice of parameters used and the benefits of using our proposed design. The conclusion is drawn in section 6.

2. Preliminaries

2.1. Dynamics of VAWTs

The dynamics modeling of a VAWT involves two parts, 1) dynamics of turbines given the resultant aerodynamic forces, and 2) aerodynamics concerning the interactions between airflow and turbine blades. Herein, the turbine dynamics will be introduced first and followed by the blade aerodynamics.

Fig. 1 shows the load analysis of a three-blade VAWT with a pitch control mechanism. Two coordinate frames are defined to explain the generation of aerodynamic forces and their applications on the turbine. The ground fixed frame is defined to have its origin located at the center of the turbine, the X-axis with a unit vector $\hat{i}$ pointing down the free wind stream, the Y-axis with a unit vector $\hat{j}$ perpendicular to the free stream, and Z-axis with a unit vector $\hat{k}$ determined by the right-hand rule. The rotation frame of each blade is defined to have its origin at the end of the arm, the normal unit vector $\hat{e}_n$ pointing towards the origin along the arms, and the tangential unit vector $\hat{e}_t$ perpendicular to $\hat{e}_n$. $\vec{U} = U\hat{i}$ is the free-stream wind.

The wind that flows across the surface of a turbine blade is a composition of local stream wind $\vec{u} = u\hat{i}$ and the induced wind due to the rotation of the turbine $\vec{V} = V\hat{e}_t = r\omega\hat{e}_t$, and it is given by

$$\vec{W} = u\hat{i} + V\hat{e}_t = W_t\hat{e}_t + W_n\hat{e}_n \tag{1}$$

where the tangential component $W_t = u\cos\theta + V$, and the normal component $W_n = u\sin\theta$, and θ is the azimuth angle. The base angle of attack α_0 due to the rotation of the turbine can be calculated by

$$\alpha_0 = \tan^{-1}\left(\frac{W_n}{W_t}\right) = \tan^{-1}\left(\frac{u\sin\theta}{u\cos\theta + V}\right) = \tan^{-1}\left(\frac{\frac{u}{U}\sin\theta}{\frac{u}{U}\cos\theta + \lambda}\right) \tag{2}$$

where λ is the tip speed ratio defined as

$$\lambda = \frac{V}{U} \tag{3}$$

For a VAWT with pitch controls, its effective angle of attack α is

$$\alpha = \alpha_0 + \delta \tag{4}$$

where δ is the pitching angle. The aerodynamic lift and drag on each blade can be calculated by using

$$\begin{cases} L = \frac{1}{2}\rho W^2 S C_L \\ D = \frac{1}{2}\rho W^2 S C_D \end{cases} \tag{5}$$

where the S is the wing area of each turbine blade (e.g., $S = ch$ for a straight blade with a chord length of c and a height of h), and C_L and C_D are the lift and drag coefficient at the angle of attack α, respectively. These coefficients are normally drawn from experimental data. The aerodynamic force can be written in its normal and tangential components as

$$\vec{F} = (L\cos\alpha + D\sin\alpha)\hat{e}_n + (L\sin\alpha - D\cos\alpha)\hat{e}_t \tag{6}$$

The torque can be calculated by using the tangential force as

$$\vec{\tau} = \vec{r}\times\vec{F} = (L\sin\alpha - D\cos\alpha)\hat{k} \tag{7}$$

Then, the torque coefficient for a single blade can be calculated by

$$C_{tb} = \frac{\tau}{\frac{1}{2}\rho A r U^2} \tag{8}$$

where A is the frontal area of the VAWT and $A = 2rh$. The instantaneous power coefficient is

$$C_{pb} = \frac{\tau\omega}{\frac{1}{2}\rho A U^3} \tag{9}$$

where ω is the angular velocity of the turbine. Due to the interference effect, the wind speed across the wind turbine is not constant; therefore, load analysis by itself is not enough to calculate the power coefficient and will be used together with fluid analysis (to be introduced in the following section) for detailed calculations of the aerodynamic forces and power coefficient.

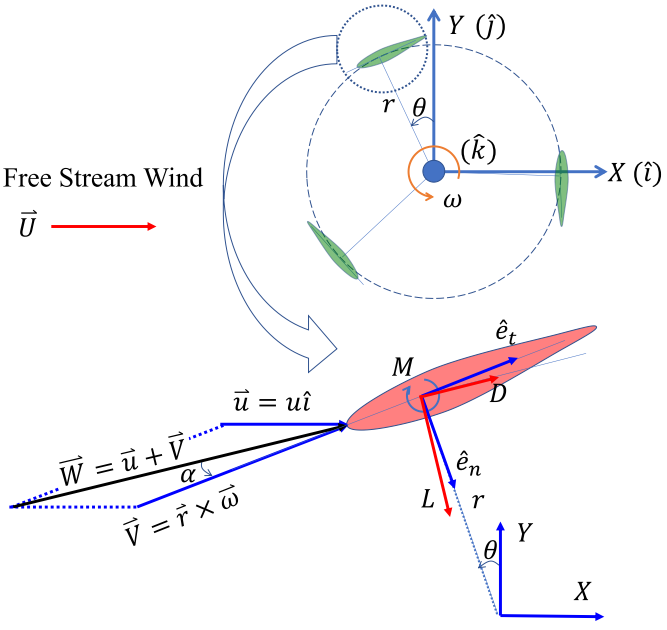

Fig. 1. Load analysis of a three-bladed VAWT with a pitch control mechanism.

2.2. Double multiple streamtube model

There are many simulation packages we can use to simulate the aerodynamics of VAWTs, including numerical models and many analytical models, such as blade element momentum theory [38], streamtube models [39–41], and vortex models [42]. For steady wind conditions, CFD-based models can provide accurate calculations for detailed flow and pressure information over the surface of turbine blades and the load distribution on the whole turbine. While CFD methods can provide more accurate flow distributions, it is too computationally expensive to be used in a real time control system. On the other side,

streamtube models divide the flow field into discretized streamtubes, and the flow within each streamtube will be summed together to give overall results. Streamtube models that can provide fast calculation of aerodynamic forces are more attractive for control system designs. Depending on how the domain is discretized, several variations studied include single streamtube (SST) [39], multiple streamtube models (MST), and double multiple streamtube models (DMST) [41]. Among these models, the DMST model divides a wind stream into upstream and downstream half-cycles for separate calculations to improve accuracy. Although DMST assumes zero expansion of the streamtubes and neglects the wake effect on blades in the downstream half-cycle, it considers the energy loss of flow throughout the upstream and downstream half-cycles. DMST provides a fairly accurate overall mean calculation, making it one of the most popular methods for the design and analysis of VAWTs. This paper focuses on improving a VAWT's performance through intelligent control, the relative improvement of the proposed method compared to existing methods is more important than the absolute accuracy of load distribution on the blades. Hence, the DMST model is used for simulating the aerodynamics behavior.

As illustrated in Fig. 2, DMST is a method based on the blade element momentum theory, it divides the rotor plane into upstream and downstream half-cycles. The flow through the turbine is discretized into N_S streamtubes (bounded by the horizontal lines), which divide the rotor circumference into $2N_S$ arcs of equal length $s = r\delta_\theta$, where $\delta_\theta = \frac{\pi}{N_S}$. Due to flow expansion, we can define the wind through the turbine in five states, including the freestream state, upstream half-cycle interaction state, equilibrium state, downstream half-cycle interaction state, and the downstream wake state. The wind speeds in these states are defined as U, u_1, u_e, u_2, and u_w, respectively.

Assuming there is no flow exchange between streamtubes, conservation of mass holds, i.e., the mass flow of each stream is constant, that is

$$\dot{m} = \rho u_1 S_1 = \rho u_2 S_2 = \text{const} \tag{10}$$

where the swept area of the streamtube i in the upstream and downstream are

$$\begin{cases} S_1 = r\delta_\theta \sin\phi, \ \text{if } \phi \in (0, \pi] \\ S_2 = r\delta_\theta(-\sin\phi), \ \text{if } \phi \in (\pi, 2\pi] \end{cases} \tag{11}$$

where ϕ is the azimuth angle of the center of the blade element in a streamtube. According to Newton's second law of motion in terms of momentum, the force exerted on the blade element throughout each half-cycle of a streamtube can be determined as

$$\begin{cases} F_1 = \dot{m}(U - u_e) \\ F_2 = \dot{m}(u_e - u_w) \end{cases} \tag{12}$$

Applying the work-energy principle, we also have

$$\begin{cases} \frac{1}{2}\dot{m}\left(u_e^2 - U^2\right) = -F_1 u_1 \\ \frac{1}{2}\dot{m}\left(u_w^2 - u_e^2\right) = -F_2 u_2 \end{cases} \tag{13}$$

Let us define the interference factor $\lambda_1 = \frac{u_1}{U}$ and $\lambda_2 = \frac{u_2}{u_e}$, then using Eqs. (12) and (13), the velocities for different states can be written in terms of the free stream velocity and interference factors as

$$\begin{cases} u_1 = \lambda_1 U \\ u_2 = (2\lambda_1 - 1)\lambda_2 U \\ u_e = (2\lambda_1 - 1)U \\ u_w = (2\lambda_2 - 1)(2\lambda_1 - 1)U \end{cases} \tag{14}$$

Combining Eqs. (12) and (14), the thrust coefficient at the streamtube can be calculated by

$$C_{F_i} = \frac{F_i}{\frac{1}{2}\rho S_i U^2} = 4\lambda_i(1 - \lambda_i), i = 1, 2 \tag{15}$$

To accommodate the inadequacy in the unidirectional flow assumption below $\lambda \approx 0.6$, Glaurt's linear modification for the thrust coefficient calculation is given by,

$$C_{Fi} = \begin{cases} \frac{1849}{900} - \frac{26\lambda_i}{15}, \ \text{if } \lambda_i < \frac{43}{60} \\ 4\lambda_i(1 - \lambda_i), \ \text{if } \lambda_i \geq \frac{43}{60} \end{cases}, \ i = 1, 2 \tag{16}$$

To solve for the interference factors, we will also need the thrust coefficient in another expression calculated from load analysis to establish a relation to the equations. Here, the lift and drag coefficients are used to calculate the instantaneous thrust each blade element receives, which is given by

$$f_i = \frac{1}{2}\rho W_i^2 c(C_L \sin\beta - C_D \cos\beta), i = 1, 2 \tag{17}$$

where c is the chord length of the blade and $\beta = \theta - \alpha$, and W_1 and W_2 are the resultant wind velocities of the blade element in the upstream and downstream half-cycles respectively. Then, the averaged thrust force in a streamtube can be calculated by

$$F_i = \frac{N_b \delta_\theta}{2\pi} f_i, i = 1, 2 \tag{18}$$

Combining Eqs. (11), (17) and (18), the thrust force coefficient of the turbine produced by the streamtube can be found by

$$\begin{cases} C_{F_1} = \dfrac{\sigma}{\pi \sin\theta} \dfrac{W_1^2}{U^2}(C_L \sin\beta - C_D \cos\beta) \\ C_{F_2} = \dfrac{-\sigma}{\pi \sin\theta} \dfrac{W_2^2}{U^2(2\lambda_1 - 1)}(C_L \sin\beta - C_D \cos\beta) \end{cases} \tag{19}$$

where σ is the solidity defined as the ratio of the blade area to the swept area of the turbine given as

$$\sigma = \frac{N_b c}{2r} \tag{20}$$

Comparing Eqs. (15) and (19), the interference factors, λ_1 and λ_2 can be calculated. With the interference factors, we can use Eqs. (1)–(9) to calculate the power coefficient of each blade. To measure the performance of the turbine, the period averaged power coefficient of a turbine with N_b blades is

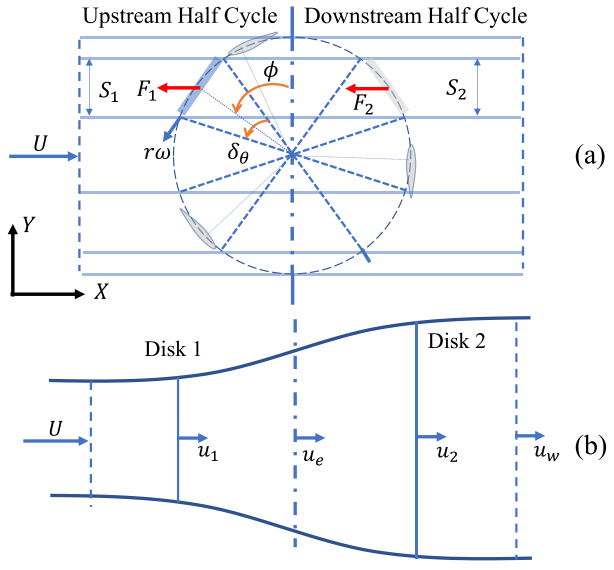

Fig. 2. Schematics of the DMST model for flow simulation (a) streamtube discretization, and (b) states of flow in a streamtube.

$$C_p = \frac{1}{2\pi}\int_0^{2\pi}\left[\sum_{i=1}^{N_b} C_{pb}\left(\theta + \frac{i-1}{N_b}2\pi\right)\right]d\theta \tag{21}$$

2.3. Dynamics and load control

The dynamics of the turbine can be obtained following Newton's second law in the form of rotational motion, given as

$$\ddot{\theta} = \left(\frac{1}{I}\right)(\tau - \tau_l) \tag{22}$$

where I is the mass moment of inertia, and τ_l is the load given as a resistive torque. A PID controller is used for load control, and the load is given by

$$\tau_l = \tau_r + k_p e + k_i \int_0^{tf} e dt + k_d \dot{e} \tag{23}$$

where the error $e = \lambda - \lambda_r$ with λ_r being the optimal tip speed ratio, and τ_r will be the reference load and has the same value of the torque at the optimal tip speed ratio.

3. Intelligent reinforcement learning control

3.1. Overall control architecture

The overall reinforcement learning control architecture is shown in Fig. 3. The system is composed of the environment and agent. The environment refers to the VAWT system in reality. In the simulation, it will be represented by a digital twin of the VAWT. The agent is the reinforcement learning controller – policy gradient with parameter exploration. It is composed of parameter updates, perturbation draws, and policy updates. Herein, the policy will be governed by the programmable four bar linkage mechanism, which provides an effective way to represent a complex pitching trajectory by only using one parameter. Details about these blocks in the architecture block diagram will be explained in the following sections.

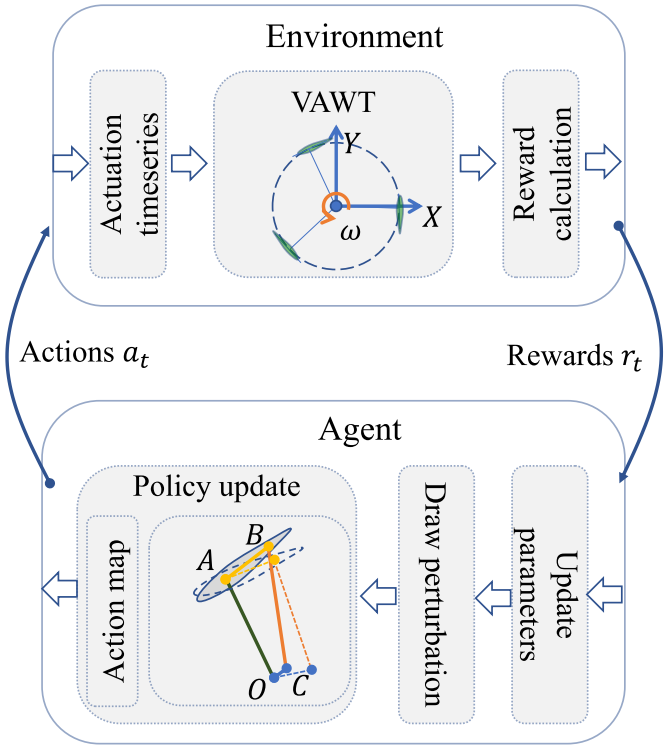

Fig. 3. The overall architecture of the proposed control system for VAWTs with an active programmable four bar linkage mechanism.

3.2. Programmable four bar linkage based pitching policy

As summarized in the literature review, the four bar linkage mechanism is one of the most promising ways for collective pitch control. Here, a programmable four bar linkage mechanism is proposed to formulate a more complex trajectory such that higher performance can be achieved. As illustrated in Fig. 4, the programmable four bar linkage mechanism is composed of the rocker OC with an adjustable length, 2 bars with fixed lengths $|OA| = r$ and AB, and the length of bar AB will be optimized to ensure that the mechanism can lead to an optimal pitching trajectory for the turbine under study. Note that, strictly speaking, the mechanism should be called a two degree of freedom (DOF) 5 bar linkage mechanism. But, since the system actively seeks for an optimal length of bar OC and it is equivalently a four bar linkage mechanism in steady state operations, we still call this mechanism a programmable four bar linkage mechanism.

From the geometric constraints between the four bars, we can establish the relationship between the input (rotation motion of bar OC) and the output pitching angel (i.e., δ), which is given by

$$\delta = \begin{cases} \beta + \gamma - \dfrac{\pi}{2}, \ if \ \dfrac{\pi}{2} \le \beta + \gamma < \dfrac{3\pi}{2} \\ \dfrac{\pi}{2} - (\beta + \gamma), \ otherwise \end{cases} \tag{24}$$

where

$$\beta = \cos^{-1}\left(\frac{l_{OA}^2 + l_{AC}^2 - l_{OC}^2}{2 l_{OA} l_{AC}}\right) \tag{25}$$

$$\gamma = \cos^{-1}\left(\frac{l_{AB}^2 + l_{AC}^2 - l_{BC}^2}{2 l_{AB} l_{AC}}\right) \tag{26}$$

$$l_{AC} = \sqrt{l_{OA}^2 + l_{OC}^2 - 2 l_{OA} l_{OC} \cos\left(\frac{\pi}{2} + \theta - \psi\right)} \tag{27}$$

Among various configurations for a four bar linkage mechanism, the drag-link configuration is suitable for this application. In this drag-link configuration, l_{oc} is the shortest link, i.e., $l_{OC} < \min\{l_{OA}, l_{AB}, l_{BC}\}$. To provide a wide range of pitching angles and avoid singularity, l_{BC} is chosen to be the longest link, i.e., $l_{BC} > \max\{l_{OA}, l_{AB}, l_{OC}\}$. Then, the following inequality need to be satisfied,

$$l_{OC} + l_{BC} \le l_{AB} + l_{OA} \tag{28}$$

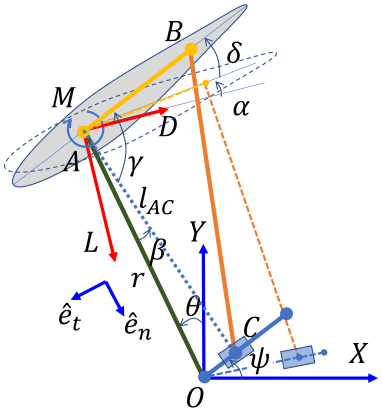

Fig. 4. Top view of a VAWT with a programmable active four bar linkage mechanism.

By changing the length of the bar *OC*, the pitching trajectory can be changed. Fig. 5 illustrates how the link lengths of l_{OC} and l_{BC} affect the pitching trajectory. A visual representation of the relationship between the length of *OC* (i.e., l_{OC}) and the corresponding pitching trajectory is shown in Fig. 5(a). We can see that the shape of the pitching angle can be significantly changed by adjusting l_{OC}. The phase shifts of the pitching trajectories can be controlled by changing the phase angle of the four bar linkage mechanism ψ. The length of the bar *BC* mainly affects the offset of the pitching trajectory. As illustrated in Fig. 5 (b), the offset of the pitching trajectory is increased from about -22° to 22° as we increase l_{BC} from 13 to 16 cm. Combining the effect from l_{OC}, l_{BC}, and ψ, more complex trajectories can be formed, a more detailed discussion will be provided in the following section.

3.3. Design optimization

A two-phase process is used to show the effectiveness of using this proposed four bar linkage mechanism for pitch control of small lift-driven vertical axis wind turbines. First, we will find the optimal tip speed ratio, optimal design of the proposed pitching mechanism (i.e., l_{AB} and l_{BC}), and optimal pitching trajectory in terms of l_{OC} by maximizing the power coefficient. Then, we will find the optimal length of the frame link l_{OC} for a wide range of operation conditions, showing that a high power coefficient can be maintained by adjusting the length of l_{OC}.

In the first phase, the pitching trajectory will be expressed in terms of l_{OC}, which is a function of the azimuth angle θ and formulated by using a general piecewise cubic spline function with uniformly distributed discretized points, i.e., $\theta_1, \cdots, \theta_{N_p} = 0 : \frac{2\pi}{N_p - 1} : 2\pi$, that is,

$$l_{OC}(\theta) = \text{spline}\big((\theta_1, x_1), \cdots, (\theta_{N_p}, x_{N_p})\big) \tag{29}$$

Let $\mathscr{P} = \{\lambda, l_{AB}, l_{BC}, \psi, x_1, \cdots, x_{N_p}\}$ be a set consisting of all the parameters to be optimized. The optimization problem can be formulated as follows,

$$arg \left(\mathscr{P} \right) \; max \; J = C_p$$
$$Subject\ to \begin{cases} l_{OC}(\theta) = spline\big((\theta_1, x_1), \cdots, (\theta_{N_p}, x_{N_p})\big) \\ x_1 = x_{N_p} \\ max(l_{OC}(\theta)\,)\langle l_{AB} < l_{OA} \\ l_{BC} > l_{OA} \\ max(l_{OC}(\theta)\,) + l_{BC} \le l_{OA} + l_{AB} \\ 0 \le \psi < 2\pi \\ \lambda_- \le \lambda \le \lambda_+ \end{cases} \tag{30}$$

where C_p is the power coefficient and a function of θ, pitching angle δ, and tip speed ratio λ. $l_{OA} = r = 12.07cm$, $N_p = 10$, $\lambda_- = 0.01$, $\lambda_+ = 3$. This optimization problem will be further solved by using nonlinear programming with the interior point algorithm, due to its ability to solve constrained optimization problems with low computational cost.

With the constraint of the four bar linkage mechanism, the pitching trajectory is constrained within a subspace. To validate the effectiveness of the proposed optimization method, we compared the result with an optimal result without the constraints of the four bar linkage mechanism. In this situation, the parameters to be optimized are $\{\lambda, x_1, \cdots, x_{N_p}\}$, the same nonlinear programming solver is used to solve the problem.

In the second phase, the optimal length of l_{OC} for tip speed ratios ranging from 0.1 to 3.0 with a step of 0.1 are found by using the optimal design found from the first phase. The optimization problem is formulated as follows,

$$\arg(l_{OC})\max J = C_P \tag{31}$$

Similar to that in phase 1, this optimization problem is also solved by using nonlinear programming with the interior point algorithm.

3.4. Online reinforcement learning control

Since our proposed programmable four bar linkage mechanism only requires one variable (i.e., length l_{OC} of the bar *OC*) to achieve complex pitching trajectory controls, it is possible to design an online reinforcement learning method to ensure the turbine can always adjust itself towards the best possible energy conversion efficiency within the subspace defined by the active programable four bar linkage mechanism. Note that, due to VAWTs' ability to omnidirectionally operate, the orientation control can be easily achieved by adjusting the constant initial phase angle (i.e., ψ) and can be done independently. Thus, it is not considered in this paper.

With the pitch control trajectory defined by the active programmable four bar linkage mechanism, it is natural to employ a policy gradient based method for online reinforcement learning control. Herein, a recently developed policy gradient with parameter exploration is used. In the PGPE algorithm, the parameter (i.e., l_{OC}) is treated as a random variable following a normal distribution $l_{OC} \sim \mathbb{N}(\mu, \sigma^2)$. Parameters μ and σ will be updated according to the history of explorative trials. As briefly mentioned in Fig. 3, in the environment-agent paradigm, the environment represents the turbine in operation, which provides rewards and observations to the agent, and according to the historical action-reward pairs $\{a_i, r_i\}$, $i = 1, \cdots, N_h$, the agent will generate a new

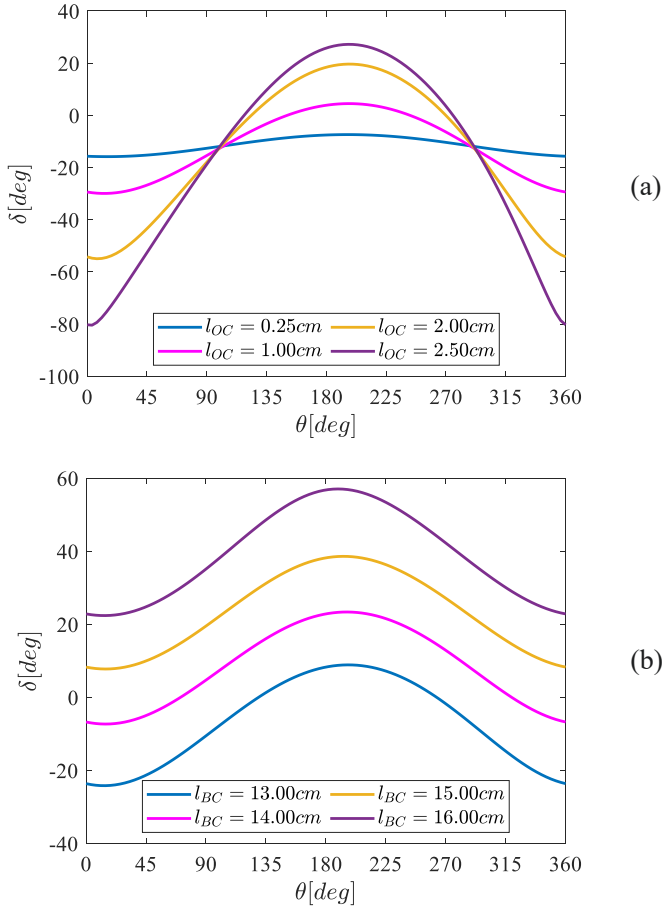

Fig. 5. Influence of link length on pitch trajectories (a) influence of l_{OC} on the pitching trajectory given $l_{OA} = 12.7cm$, $l_{AB} = 0.75c = 3.81cm$, and $l_{BC} = 13.97cm$, and (b) influence of l_{BC} on the pitching trajectory given $l_{OA} = 12.7cm$, $l_{AB} = 0.75c = 3.81cm$, and $l_{OC} = 0.3937cm$.

action a_t. Under steady wind conditions, since the states of a VAWT are fully determined by the previous state and action, and the control action only depends on the current state and the parameter, the requirements of PGPE for the system to be Markovian and stochastic policy suffice. The expected rewards with given parameters $\varrho = \{\mu, \sigma\}$ can be written as the following double integral over the whole history space $\mathscr{H}$ and parameter space Θ,

$$J(\varrho) = \int_{\Theta}\int_{\mathscr{H}} p(\vartheta, \xi|\varrho) r(\vartheta) d\vartheta d\xi \tag{32}$$

where $p(\vartheta, \xi|\varrho)$ is the joint probability of a state-action pair history $\vartheta = \{a_i, r_i\}, i = 1, \cdots, N_h$, and a random parameter draw ξ given parameters ϱ, and $r(\vartheta) = \sum_{t=1}^{N_h} r_t$ represents the cumulative reward over history (e.g., a cumulative reward for a whole rotation cycle $\theta \to 0 \sim 2\pi$). The gradient of $J(\varrho)$ can be written as

$$\nabla_{\varrho} J(\varrho) = \int_{\Theta}\int_{\mathscr{H}} \nabla_{\varrho} p(\vartheta, \xi|\varrho) r(\vartheta) d\vartheta d\xi \tag{33}$$

Since $\nabla_{\varrho} p(\vartheta, \xi|\varrho) = p(\vartheta, \xi|\varrho) \nabla_{\varrho} \log p(\vartheta, \xi|\varrho)$, and ϑ is conditionally independent of ϱ given a random draw ξ (i.e., $p(\vartheta, \xi|\varrho) = p(\xi|\varrho) p(\vartheta|\xi)$), Eq. (33) can be written as

$$\begin{aligned} \nabla_{\varrho} J(\varrho) &= \int_{\Theta}\int_{\mathscr{H}} \nabla_{\varrho} p(\vartheta, \xi|\varrho) r(\vartheta) d\vartheta d\xi \\ &= \int_{\Theta}\int_{\mathscr{H}} p(\vartheta, \xi|\varrho) \nabla_{\varrho} \log p(\vartheta, \xi|\varrho) r(\vartheta) d\vartheta d\xi \\ &= \int_{\Theta}\int_{\mathscr{H}} p(\xi|\varrho) p(\vartheta|\xi) \nabla_{\varrho} \begin{pmatrix} \log p(\vartheta|\xi) \\ +\log p(\xi|\varrho) \end{pmatrix} r(\vartheta) d\vartheta d\xi \\ &= \int_{\Theta}\int_{\mathscr{H}} p(\xi|\varrho) p(\vartheta|\xi) \nabla_{\varrho} \log p(\xi|\varrho) r(\vartheta) d\vartheta d\xi \end{aligned} \tag{34}$$

Since integrating over the entire space is not realistic in practice, the sampling method can be applied to find a gradient estimator. Starting with a random draw ξ from $p(\xi|\varrho)$, ξ is applied to generate a history ϑ from $p(\vartheta|\xi)$. Then, the discrete approximator of Eq. (34) can be written as

$$\nabla_{\varrho} J(\varrho) = \frac{1}{H} \sum_{t=1}^{H} \nabla_{\varrho} \log p(\xi|\varrho) r(\vartheta_t) \tag{35}$$

where H is the length of history. Since $\varrho = \{\mu, \sigma\}$ and $\xi \in \mathbb{N}(\mu, \sigma)$, assuming all parameters in ξ are independent, i.e., $\xi_i \in \mathbb{N}(\mu_i, \sigma_i)$, we have

$$p(\xi_i|\varrho) = \frac{1}{\sqrt{2\pi}\sigma_i} e^{-\frac{(\xi_i - \mu_i)^2}{2\sigma_i^2}} \tag{36}$$

and further, we can find

$$\begin{cases} \nabla_{\mu_i} \log p(\xi_i|\varrho) = \dfrac{\xi_i - \mu_i}{\sigma_i^2} \\ \nabla_{\sigma_i} \log p(\xi_i|\varrho) = \dfrac{(\xi_i - \mu_i)^2 - \sigma_i^2}{\sigma_i^3} \end{cases} \tag{37}$$

Although this approximation can approach arbitrary accuracy given enough samples, a lighter version of the gradient estimator by sampling with a baseline is used to update the parameters. If the step size a_i is chosen as $a\sigma_i^2$ in a positive gradient direction, the parameters can be updated by

$$\begin{cases} \Delta\mu_i = a(r_t - b)(\theta_i - \mu_i) \\ \Delta\sigma_i = a(r_t - b)\dfrac{(\theta_i - \mu_i)^2 - \sigma_i^2}{\sigma_i} \end{cases} \tag{38}$$

Let us define the reward history $r = [r_t - b]^T$, the history of offsets from the mean value in random draws $T = [T_{i,t}] = [\xi_{i,t} - \mu_i]$, and the history of deviations of random draws $S = [S_{i,t}] = \left[\frac{(\xi_{i,t} - \mu_i)^2 - \sigma_i^2}{\sigma_i}\right]$, then, the parameter update law can be further written in the following compact form as

$$\begin{cases} \mu \leftarrow \mu + aTr \\ \sigma \leftarrow \sigma + aSr \end{cases} \tag{39}$$

To reduce the dependence of convergence on the absolute value of the difference between the reward and the baseline, normalization is used when updating the parameters, given by,

$$\begin{cases} \mu \leftarrow \mu + \dfrac{a}{m - b} Tr \\ \sigma \leftarrow \sigma + \dfrac{a}{m - b} Sr \end{cases} \tag{40}$$

4. Results

4.1. Simulation setup

Simulation is used to verify the effectiveness of the proposed pitch control mechanism and intelligent control algorithm of the VAWT sketched in Fig. 6. The simulation is based on a 2D model due to its good accuracy in calculating aerodynamic forces for blades with high aspect ratios. Although a 3D model considers the tip vortex effect and provides a more realistic simulation, it comes with a higher computational cost. Moreover, the control strategy is based on the measurement of the coefficient of power, the choice between a 2D or 3D model doesn't affect how the control system works. The program made for optimizing the four bar linkage was written using MATLAB. The aerodynamics is simulated using the DMST model. The implementation of the DMST model is developed in the package "VAWT Analysis" by David Vallverdu written using MATLAB [43]. Note that the calculations are based on the lift and drag coefficients calculated from XFOIL, the power coefficient values are good for relative comparison, but the values may be different if more accurate or experimental lift and drag coefficients are used. The learning rate used for all tests is 0.02.

The main features of the VAWT used in this paper are provided in Table 1. Simulation is used to verify the effectiveness of the proposed active pitch control system.

4.2. Pitch mechanism optimization

To show how well the pitch mechanism can form pitching trajec-

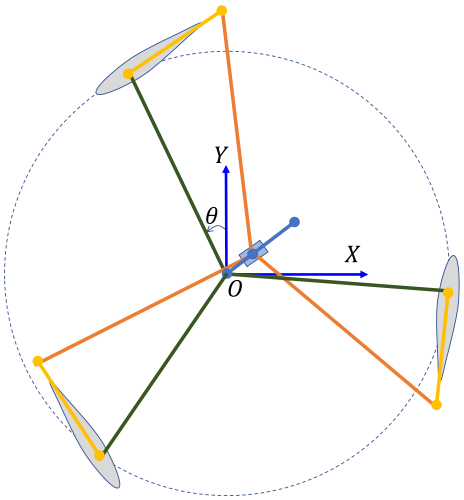

Fig. 6. Top view sketch of the VAWT.

Table 1
Main features of the VAWT.

Rotor Radius (l_{OA}) [cm]	12.07
Height (h) [cm]	25.4
Blade number (N_b)	3
Airfoil profile	NACA 0021
Length of link AB (l_{AB}) [cm]	5.08

tories, we first find the global optimal pitching trajectory without considering the constraint from the four bar linkage mechanism, and the result is given in Fig. 7. It can be seen that a maximum power coefficient of 44.11% is achieved with an optimal tip speed ratio $\lambda = 1.722$.

The comparison between the optimal pitching trajectory found by using the proposed method to the global optimum is given in Fig. 8. Here, in Fig. 8(a) we can see that the two pitching trajectories are very similar. The maximum power coefficient is 38.57%, which is only 5.54% less than the global optimal results. The optimal tip speed ratio is $\lambda = 1.59$. The optimal four bar linkage design is found to have $l_{AB} = 8.90$ cm, $l_{BC} = 14.98$ cm, $\psi = 261.42$ degrees. From Fig. 8(b), we can see that the trajectory of l_{OC} varies smoothly between 1 cm and 4 cm as a function of θ and can be controlled by using a linear motor or motor driven lead screw.

The optimal length of l_{OC} for a wide range of tip speed ratios are shown in Fig. 9(a). The optimal power coefficient is found to be 26.10% with $\lambda = 1.87$ and $l_{OC} = 2.10$ cm with a pitch trajectory shown in Fig. 8 (b). It is important to note that the optimal l_{OC} decreases monotonically as tip speed ratio increases. This will ensure the optimum can always be obtained and the result is unique.

4.3. System performance

The proposed VAWT design with an active programmable four bar linkage mechanism and the corresponding control system is tested under both constant and varying wind conditions. Since the turbine's response to wind direction changes can be easily accommodated by adjusting the initial phase angle of the turbine, only wind speed changes are considered in this study.

Case I. System performance under a constant tip speed ratio. Fig. 10 shows the system's performance under a tip speed ratio of 1.87, which is also the optimal tip speed ratio for operation. In this case, the wind speed is set to 10 m/s, and the distribution of the frame link length l_{OC} is initialized as Gaussian with a mean of 3.31 cm and a standard deviation of 0.5 cm. These initial values were purposely chosen to have a

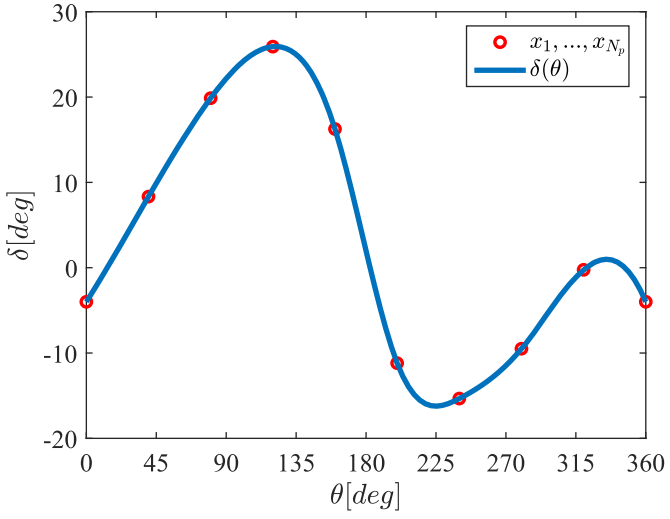

Fig. 7. Optimal pitching trajectory without the four bar linkage mechanism (optimal $\lambda = 1.722$ with $C_p = 44.11\%$).

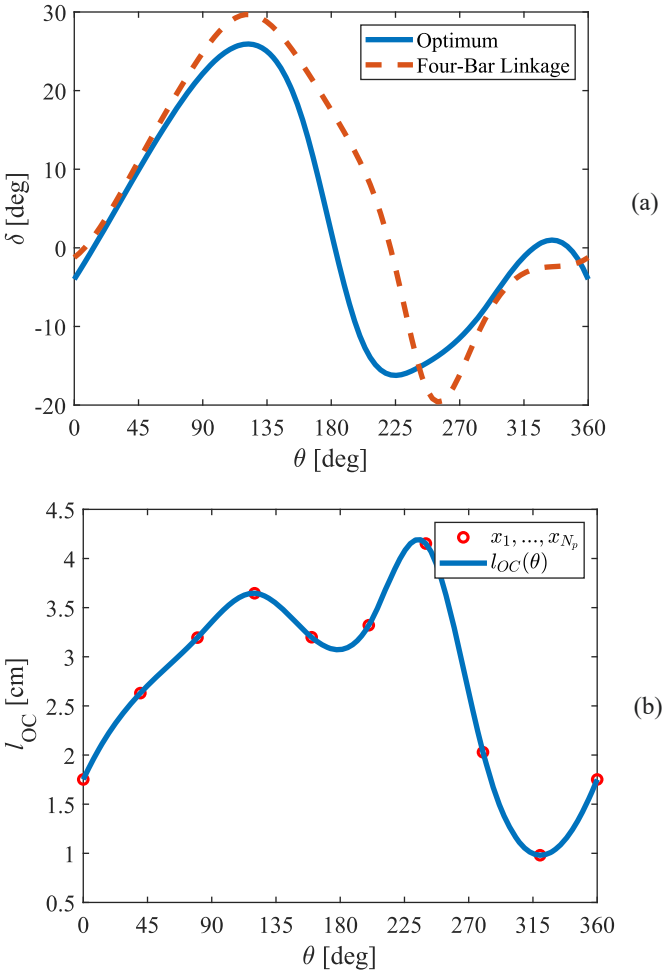

Fig. 8. Comparison of the optimal pitching trajectory from the four bar linkage mechanism with the globally optimal result (a) pitching trajectory, and (b) trajectory of l_{OC}.

discrepancy from the optimal solution $l_{OC} = 2.07$ cm as shown in Fig. 9. The mean and standard deviation of the parameter l_{OC} are both updated after each episode according to the history of rewards in 10 cycles. The reward is defined as the mean of the power coefficient in a cycle. The convergence is found when the changes in the mean (blue dots) and the standard deviation (shaded purple area) stagnate. We can see that the system converges to an optimal power coefficient of 0.261 in about 60 episodes, which is equivalent to 25.61 s in reality at a rotational speed of 147.15 rad/s.

After that, we further test the system's performance under a wide range of wind conditions with the tip speed ratio ranging from 0.1 to 3. The histories of the rewards and length of l_{OC} are shown in Fig. 11. Similar trends to that in Fig. 10 can be observed for these tests under varying wind conditions. In all tests, we see the baseline rewards and the distribution of l_{OC} converge. It can be seen that the system can always converge to an optimal power coefficient within 100 episodes, which is 42s at optimal tip speed ratio seconds in real time. Here, the initial guesses for all cases are given as the midlength of $l_{OC} = 3.31$ cm to show the effectiveness of the algorithm. Carefully selected initial guesses can result in a faster convergence rate. This effect is observed for the test with a tip speed ratio of 1.2 where the initial length is nearest to its optimum.

Case II. Startup performance under a constant wind speed of 10 m/s. Self-starting capabilities have been an issue for VAWTs without a pitch control mechanism, here, the start-up performance under a constant wind speed of 10 m/s is given in Fig. 12. Using the same initial

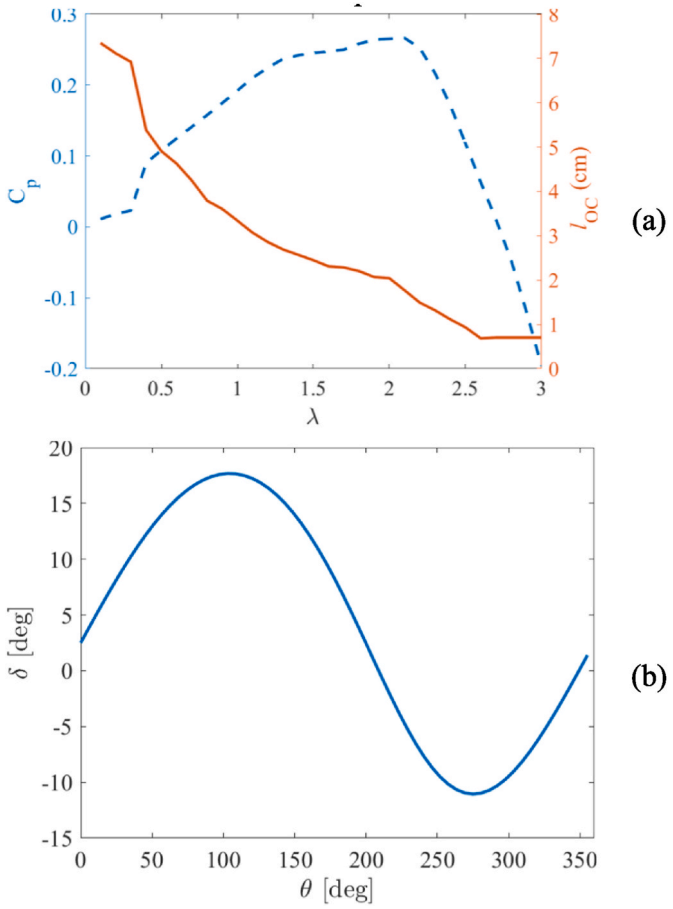

Fig. 9. (a) Optimal l_{OC} and power coefficient for $\lambda = 0.1 \sim 3$, and (b) optimal pitching trajectory at $\lambda = 1.76$.

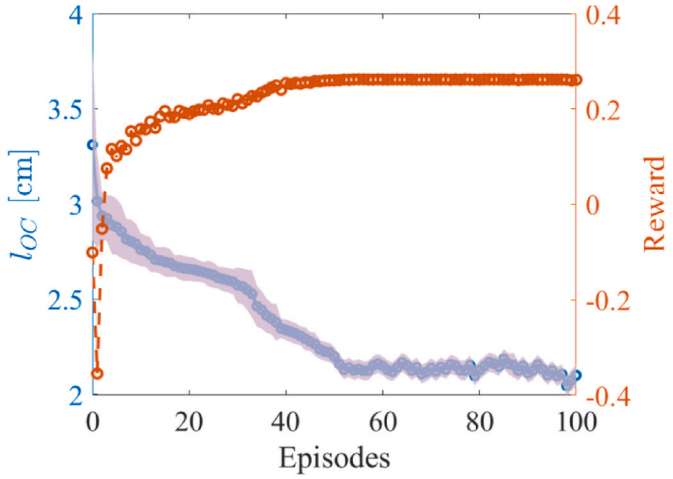

Fig. 10. Performance under a constant wind speed with histories of l_{OC} and reward.

parameters as those in tests of Case I, we can observe the turbine has the self-starting capability in contrast with fixed pitch VAWTs which have low and negative power coefficients at low tip speed ratios. As we can see that the maximum reward (power coefficient) can be reached in 35 episodes, which is equivalently 15.2 s in reality.

Case III. System performance under varying wind conditions. This case simulates the performance of wind turbines from the start to tracking under varying wind conditions. Since the public wind data from weather stations are recorded every several minutes, the system converges long before the next wind data point is available, making it difficult to see the transient behavior. Hence, instead of using those data, artificial wind information shown in Fig. 13(a) is used to test the effectiveness of the proposed pitch control system. The wind profile captures a type of wind speed change cycle from a medium speed of 15.73 m/s to a relatively high speed of about 18.49 m/s and later slows down to 7.08 m/s. From Case II, the proposed control system converges in about 35 episodes (i.e., 350 cycles), which is equivalently 12 s in reality. This will allow us to test the performance of the system more thoroughly since more variations will be experienced within a much short time. If this system works under this condition, it implies the system will work in the reality.

4.4. Comparison to other methods

To further validate the improvement of the proposed system, its performance is further compared to a turbine with the same configuration but with a constant pitch angle of 5°, and another identically configured turbine with a passive four bar linkage mechanism for pitch control with a frame link length of $l_{OC} = 1.5$ cm, which will be used as the initial value of our system as well. The comparison of the operation of the three VAWTs at a wide range of tip speed ratios of $\lambda = \{0.1, 0.6, 1.2, 1.8, 2.4, \text{and } 3.0\}$ is shown in Fig. 14. We can see (1) for both four bar linkage systems, they can hold a positive coefficient of power throughout a broad band of tip speed ratios; however, the system with online reinforcement learning controls is always able to have a higher performance; (2) the turbine with a constant pitch has a negative power coefficient for a wide range of tip speed ratios, implying the turbine doesn't have the self-starting capability; (3) both the turbine with a passive four bar linkage mechanism and ours have self-starting capability since their power coefficient is always positive, and our method performs much better than that of the system with a passive four bar linkage pitching mechanism; and (4) the turbine with a passive four bar linkage pitching mechanism only has a good performance at a specific tip speed ratio (e.g., $\lambda = 1.8$), which is inherited from the design and it has a poor performance outside a very small region near the designed optimal operation point; and (5) our proposed design actively seeks for the optimal design within a subspace defined by pitching mechanism; hence, the best possible performance can be maintained regardless of the tip speed ratios.

The transient performance of the three VAWTs is also compared and the results are shown in Fig. 15. All three turbines use the same load controller. The passive four bar linkage pitching mechanism is assumed to have a fixed frame link of 1.5 cm. We can see that the turbine with a fixed pitching angle (colored in yellow) is not able to self-start, the power coefficient has a peak at the beginning and then drops rapidly to about 0.07 and stays there. The turbine with a passive four bar linkage mechanism can reach the optimal tip speed ratio fairly quickly within 1 s and reaches a maximum power very fast with some overshoot and then settles down at a constant $C_p = 0.20$. Although it takes our system a longer time of about 15 s to reach a maximum power coefficient and the desired tip speed ratio compared to the turbine with a passive four bar linkage mechanism, our proposed system can reach a much higher power coefficient of 0.261, which represents a 30.5% increase.

5. Discussion

One of the contributions made in this paper is a description of a variable pitching trajectory by using only one parameter, which is the length of the frame link of the four bar linkage mechanism. For a static wind environment, increasing the number of parameters for describing the pitch trajectory gives it a more flexible representation. This may lead to an increase in the ultimate coefficient of power. However, in a dynamically changing urban wind environment, the primary goal is to shorten the convergence time such that the pitch control can adapt

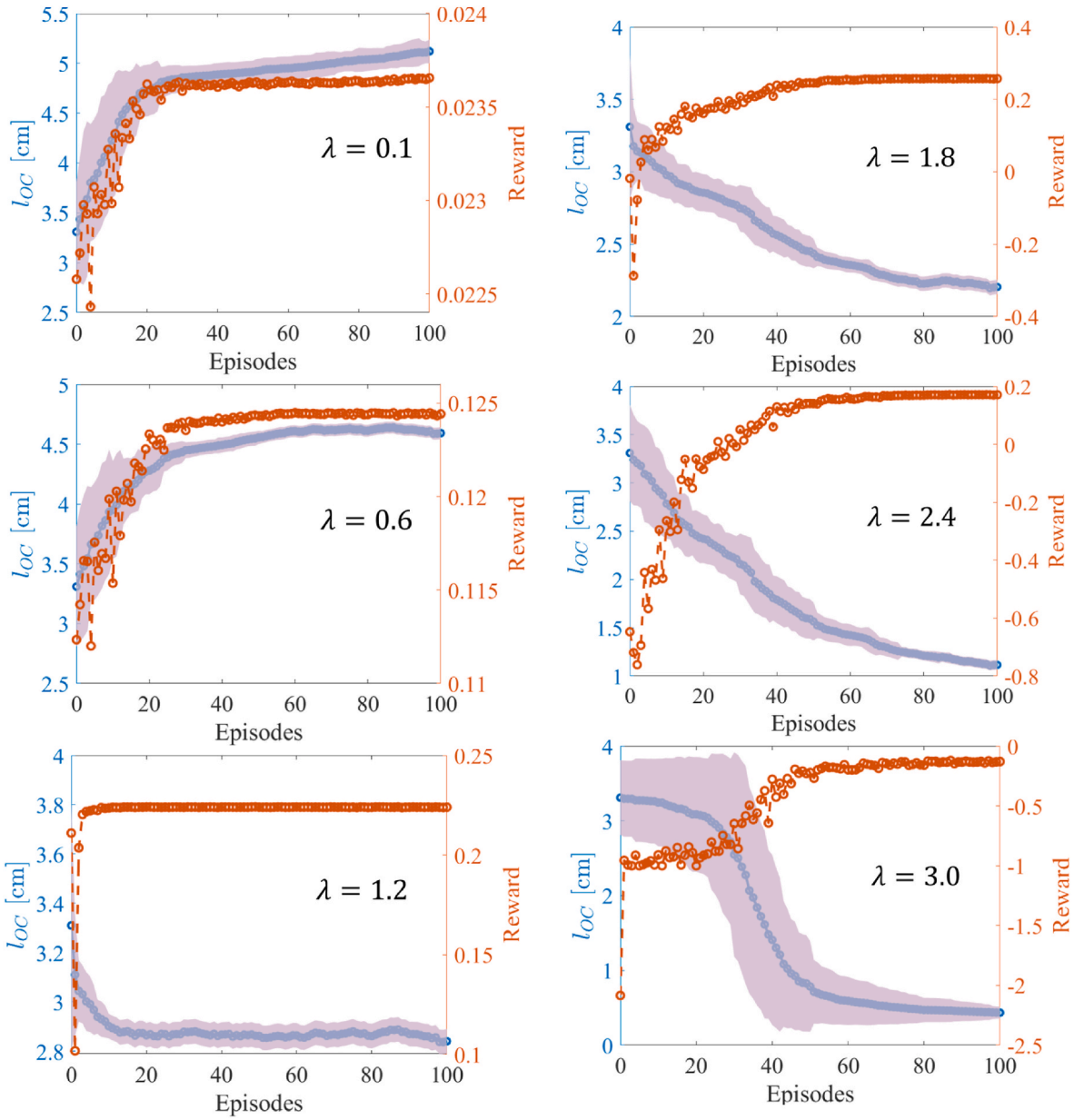

Fig. 11. Performance under constant wind speeds with tip speed ratios of 0.1, 0.6, 1.2, 1.8, 2.4, and 3.0.

quickly to the wind changes to maintain a high performance. Hence, we minimize the parameters for the control policy.

Besides the control policy parameters, we also consider the parameters pertaining to the wind conditions, including the wind speed, direction, fluctuation frequency, and fluctuation amplitude. According to the work from Chen et al. [16], tip speed ratio was the dominant factor which impacted the performance of a turbine. Given an operation state, the tip speed ratio only depends on the wind speed, which is the wind parameter considered in this paper. Also, due to the omnidirectional operation capability, VAWTs do not need a complex steering mechanism like HAWTs to turn the turbine into the wind. Accommodations to wind direction changes are done by applying a phase shift to the pitching control commands. This can be done instantaneously, and therefore will not affect the pitching control.

The proposed method relies on the measurements of the power coefficient to adjust the governing parameter (i.e. length of the frame link) of the pitch trajectory. This control method works regardless of the choice in airfoil shape. The symmetric airfoil NACA 0021 is selected for demonstration due to its wide utilization in existing literature. The proposed system also works for turbines with asymmetric airfoils and can be seen as a method to boost the performance of VAWTs without an effective and adaptive pitch control mechanism.

6. Conclusion

This paper presents a VAWT design with an active programmable four bar linkage mechanism and online reinforcement learning control method to help VAWTs maintain high power generation under changing wind environment. High performance is achieved by controlling the pitching angles of the blade to follow an iteratively updated control policy. The iterative process governed by reinforcement learning ensures the parameters are updated towards an increasing coefficient of power. The proposed design significantly reduced the number of parameters needed to describe a complex pitch trajectory by constraining the trajectories in a subspace governed by the kinematics of a four bar linkage mechanism. The optimized design allows the system to reach and maintain a high power coefficient for a wide range of tip speed ratios. Due to the great reduction in the number of parameters, the

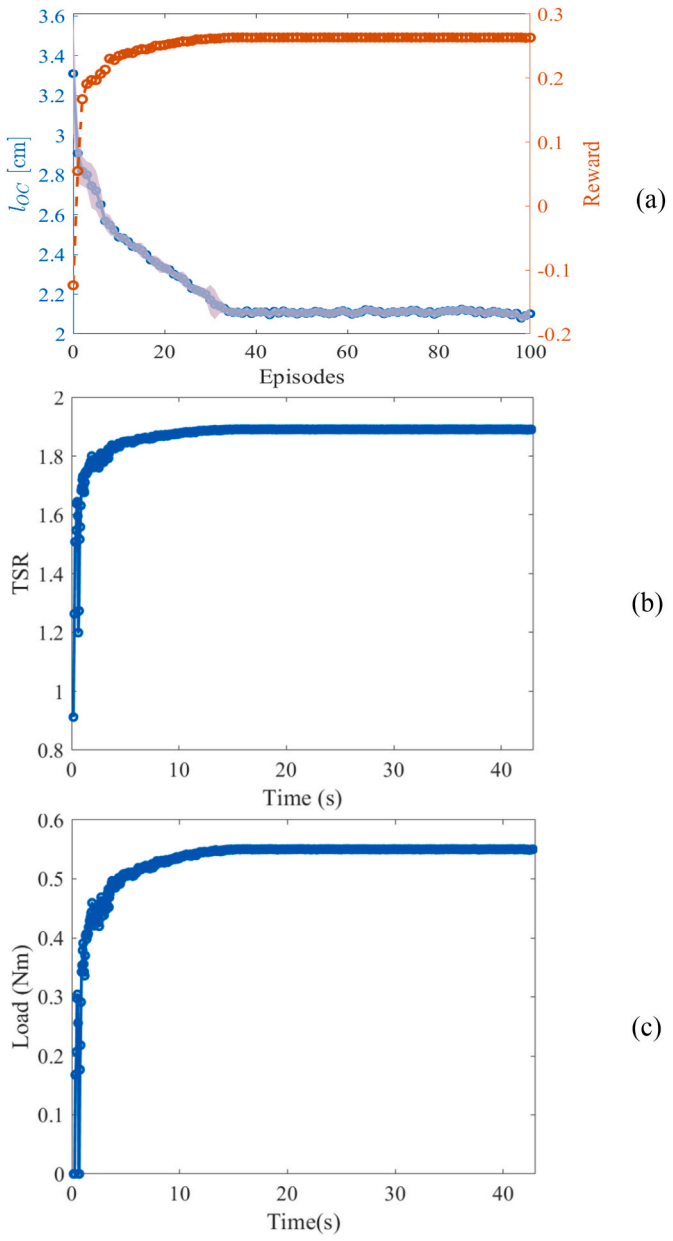

Fig. 12. Startup performance with pitch and load control (a) histories of reward and l_{OC}, (b) tip speed ratio (TSR), and (c) load.

maximum power coefficient can be achieved by the reinforcement learning algorithm within a short time, which makes it appropriate to be implemented in reality. By comparing both the steady state and transient performance of our proposed system to another two identically configured turbines, one with a fixed pitch angle and the other with a passive pitch control mechanism, we demonstrated that the proposed design can always achieve a much higher power coefficient. It is also demonstrated that, by using a varying length in the frame link, the self-starting capability is enabled and a power coefficient close to the global optimum can be maintained for complex and dynamically changing wind environments.

Credit author statement

He Shen contributed to the conceptualization and methodology used in the paper. He developed the fundamental theories and formulated the framework of the research. He also contributed to the writing, validation, and editing. Alexis Ruiz contributed to the theories and simulation

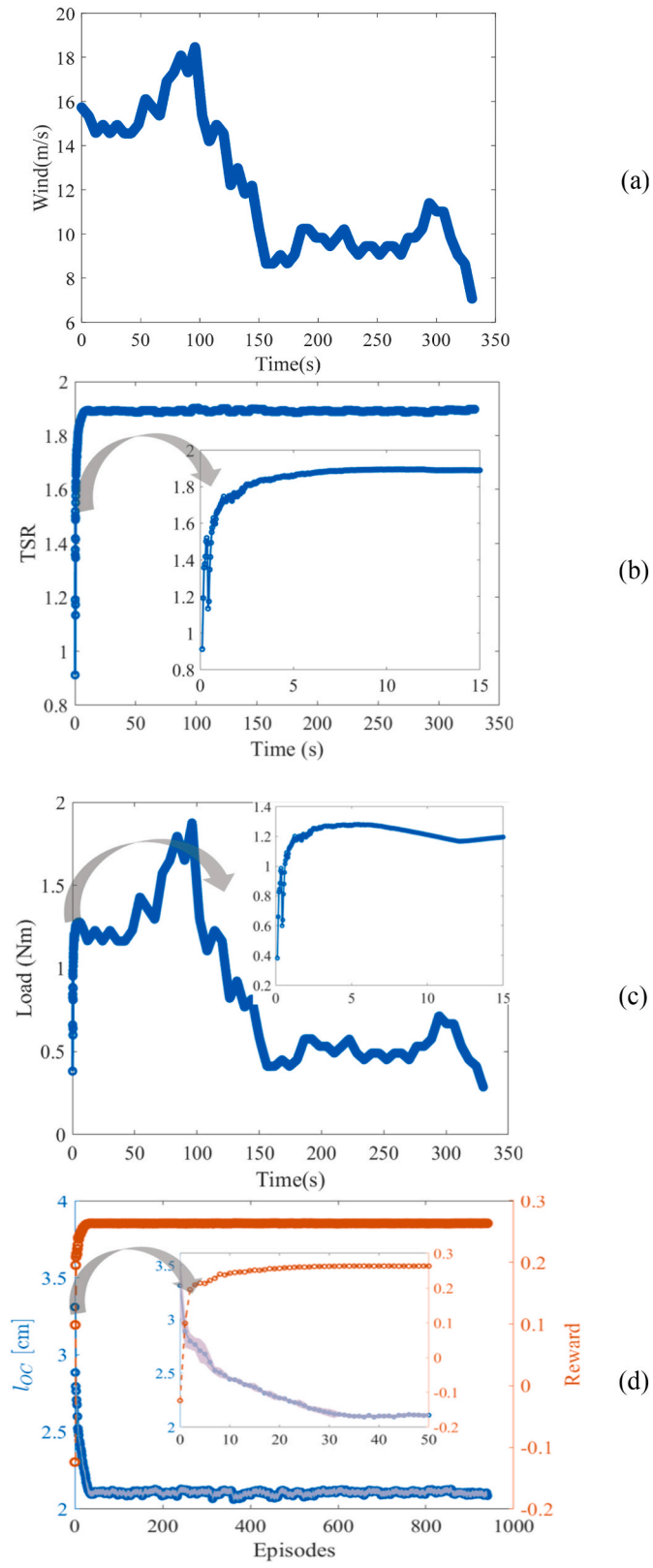

Fig. 13. System performance under varying wind conditions (a) wind profile, (b) tip speed ratio (TSR) including transient response, (c) the load control including the transient response, (d) history of reward and frame-link length l_{OC} with a focused view of the transient response.

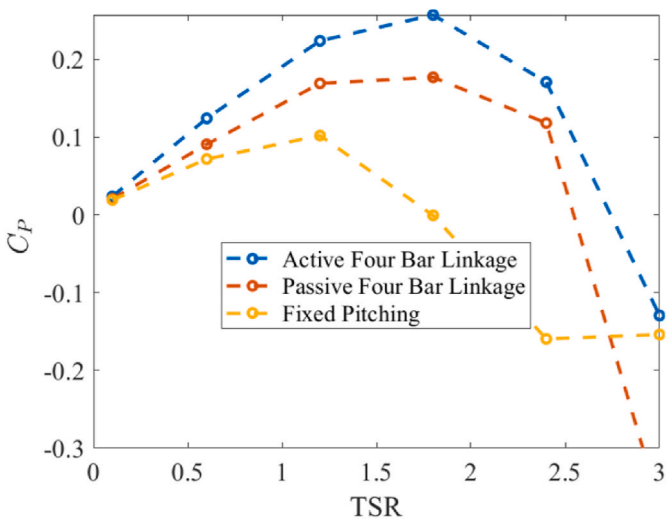

Fig. 14. Comparison in system performance between our method, passive four bar linkage pitching mechanism, and a fixed pitch angle at tip speed ratios of 0.1, 0.6, 1.2, 1.8, 2.4, and 3.0.

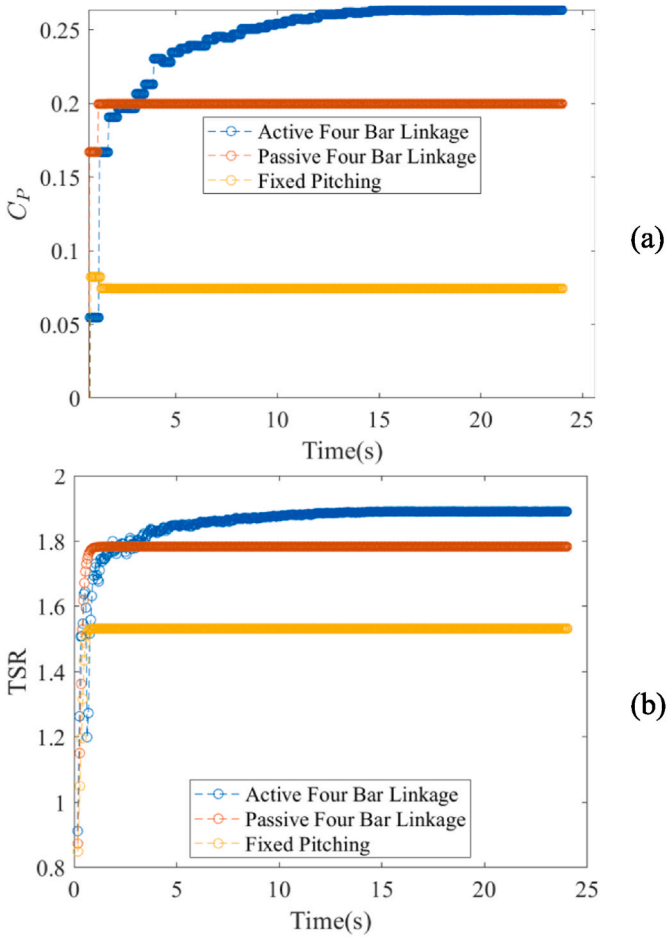

Fig. 15. Comparison of the transient behavior (a) power coefficient, (b) tip speed ratio (TSR).

and prepared most of the results. He also contributed to the writing and revision of the paper. Ni Li contributed to the formulation of the research idea and methodology. She developed and validated the theories used in this work and contributed to the writing and proofreading of the paper.

Declaration of competing interest

The authors declare that they have no known competing financial interests or personal relationships that could have appeared to influence the work reported in this paper.

Data availability

Data will be made available on request.

Acknowledgments

This work has been partially supported by the National Science Foundation with Award No. HRD-1547723, OAC- 1835727. Alexis Ruiz is the recipient of a CREST-CEaS fellowship, for which we are grateful.

Appendix A. Supplementary data

Supplementary data to this article can be found online at https://doi.org/10.1016/j.energy.2022.125350.

References

[1] Abdolahifar A, Karimian SMH. A comprehensive three-dimensional study on Darrieus vertical axis wind turbine with slotted blade to reduce flow separation. Energy 2022;248:123632. https://doi.org/10.1016/j.energy.2022.123632.
[2] Celik Y, Ingham D, Ma L, Pourkashanian M. Design and aerodynamic performance analyses of the self-starting H-type VAWT having J-shaped aerofoils considering various design parameters using CFD. Energy 2022;251:123881. https://doi.org/10.1016/j.energy.2022.123881.
[3] Eriksson S, Bernhoff H, Leijon M. Evaluation of different turbine concepts for wind power. Renew Sustain Energy Rev 2008;12:1419–34. https://doi.org/10.1016/j.rser.2006.05.017.
[4] Zhao Z, Wang D, Wang T, Shen W, Liu H, Chen M. A review: approaches for aerodynamic performance improvement of lift-type vertical axis wind turbine. Sustain Energy Technol Assessments 2022;49:101789. https://doi.org/10.1016/j.seta.2021.101789.
[5] Almohammadi KM, Ingham DB, Ma L, Pourkashanian M. 2-D-CFD analysis of the effect of trailing edge shape on the performance of a straight-blade vertical axis wind turbine. IEEE Trans Sustain Energy 2015;6:228–35. https://doi.org/10.1109/TSTE.2014.2365474.
[6] Jo Dabiri. Potential order-of-magnitude enhancement of wind farm power density via counter-rotating vertical-axis wind turbine arrays. J Renew Sustain Energy 2011;3. https://doi.org/10.1063/1.3608170.
[7] Zhao Z, Wang R, Shen W, Wang T, Xu B, Zheng Y, et al. Variable pitch approach for performance improving of straight-bladed VAWT at rated tip speed ratio. Appl Sci 2018;8. https://doi.org/10.3390/app8060957.
[8] Kirke BK, Lazauskas L. Experimental verification of a mathematical model for predicting the performance of a self-acting variable pitch vertical axis wind turbine. Wind Eng 1993:58–66.
[9] Li Q, Cai C, Maeda T, Kamada Y, Shimizu K, Dong Y, et al. Visualization of aerodynamic forces and flow field on a straight-bladed vertical axis wind turbine by wind tunnel experiments and panel method. Energy 2021;225:120274. https://doi.org/10.1016/j.energy.2021.120274.
[10] Syawitri TP, Yao YF, Chandra B, Yao J. Comparison study of URANS and hybrid RANS-LES models on predicting vertical axis wind turbine performance at low, medium and high tip speed ratio ranges. Renew Energy 2021;168:247–69. https://doi.org/10.1016/j.renene.2020.12.045.
[11] Islam M, Ting DSK, Fartaj A. Desirable airfoil features for smaller-capacity straight-bladed VAWT. Wind Eng 2007;31:165–96. https://doi.org/10.1260/030952407781998800.
[12] Zhang Y, Guo Z, Zhu X, Li Y, Song X, Cai C, et al. Investigation of aerodynamic forces and flow field of an H-type vertical axis wind turbine based on bionic airfoil. Energy 2022;242:122999. https://doi.org/10.1016/j.energy.2021.122999.
[13] Tian W, Ni X, Mao Z, Wang YF. Study on the performance of a new VAWT with overlapped side-by-side Savonius rotors. Energy Convers Manag 2022;264:115746. https://doi.org/10.1016/j.enconman.2022.115746.
[14] Cuevas-Carvajal N, Cortes-Ramirez JS, Norato JA, Hernandez C, Montoya-Vallejo MF. Effect of geometrical parameters on the performance of conventional Savonius VAWT: a review. Renew Sustain Energy Rev 2022;161:112314. https://doi.org/10.1016/j.rser.2022.112314.
[15] Peng HY, Zhong BW, Hu G, Liu HJ. Optimization analysis of straight-bladed vertical axis wind turbines in turbulent environments by wind tunnel testing. Energy Convers Manag 2022;257. https://doi.org/10.1016/j.enconman.2022.115411.
[16] Chen WH, Wang JS, Chang MH, Tuan Hoang A, Shiung Lam S, Kwon EE, et al. Optimization of a vertical axis wind turbine with a deflector under unsteady wind conditions via Taguchi and neural network applications. Energy Convers Manag 2022;254:115209. https://doi.org/10.1016/j.enconman.2022.115209.

[17] Santamaría L, Fernández Oro JM, Argüelles Díaz KM, Meana-Fernández A, Pereiras B, Velarde-Suárez S. Novel methodology for performance characterization of vertical axis wind turbines (VAWT) prototypes through active driving mode. Energy Convers Manag 2022;258. https://doi.org/10.1016/j.enconman.2022.115530.
[18] Roy S, Saha UK. Wind tunnel experiments of a newly developed two-bladed Savonius-style wind turbine. Appl Energy 2015;137:117–25. https://doi.org/10.1016/j.apenergy.2014.10.022.
[19] Ricci R, Romagnoli R, Montelpare S, Vitali D. Experimental study on a Savonius wind rotor for street lighting systems. Appl Energy 2016;161:143–52. https://doi.org/10.1016/j.apenergy.2015.10.012.
[20] Liu K, Yu M, Zhu W. Enhancing wind energy harvesting performance of vertical axis wind turbines with a new hybrid design: a fluid-structure interaction study. Renew Energy 2019;140:912–27. https://doi.org/10.1016/j.renene.2019.03.120.
[21] Kuang L, Su J, Chen Y, Han Z, Zhou D, Zhang K, et al. Wind-capture-accelerate device for performance improvement of vertical-axis wind turbines: external diffuser system. Energy 2022;239:122196. https://doi.org/10.1016/j.energy.2021.122196.
[22] Shukla V, Kaviti AK. Performance evaluation of profile modifications on straight-bladed vertical axis wind turbine by energy and Spalart Allmaras models. Energy 2017;126:766–95. https://doi.org/10.1016/j.energy.2017.03.071.
[23] Sun X, Zhu J, Li Z, Sun G. Rotation improvement of vertical axis wind turbine by offsetting pitching angles and changing blade numbers. Energy 2021;215:119177. https://doi.org/10.1016/j.energy.2020.119177.
[24] Benedict M, Lakshminarayan V, Pino J, Chopra I. Aerodynamics of a small-scale vertical-Axis wind turbine with dynamic blade pitching. AIAA J 2016;54:924–35. https://doi.org/10.2514/1.J052979.
[25] Zhang L, Zhang S, Wang K, Liu X, Liang Y. Study on synchronous variable-pitch vertical axis wind turbine. 2011 Asia-Pacific Power. Energy Eng. Conf. 2011:1–5. https://doi.org/10.1109/appeec.2011.5748440.
[26] Sagharichi A, Maghrebi MJ, Arabgolarcheh A. Variable pitch blades : an approach for improving performance of Darrieus wind turbine. J Renew Sustain Energy 2016;8. https://doi.org/10.1063/1.4964310.
[27] Kiwata T, Yamada T, Kita T. Performance of a vertical axis wind turbine with variable-pitch straight blades utilizing a linkage mechanism. J Environ Eng 2010;5:213–25. https://doi.org/10.1299/jee.5.213.
[28] Elkhoury M, Kiwata T, Aoun E. Experimental and numerical investigation of a three-dimensional vertical-axis wind turbine with variable-pitch. J Wind Eng Ind Aerod 2015;139:111–23. https://doi.org/10.1016/j.jweia.2015.01.004.
[29] Rathore MK, Agrawal M, Baredar P. Pitch control mechanism in various type of vertical axis wind turbines: a review. J Vib Eng Technol 2021;9:2133–49. https://doi.org/10.1007/s42417-021-00352-4.
[30] Hand MM, Balas MJ. Systematic controller design methodology for variable-speed wind turbines. Wind Eng 2000;24:169–87. https://doi.org/10.1260/0309524001495549.
[31] Camblong HÃ. Digital robust control of a variable speed pitch regulated wind turbine for above rated wind speeds. Control Eng Pract 2008;16:946–58. https://doi.org/10.1016/j.conengprac.2007.11.004.
[32] Moradi H, Vossoughi G. Robust control of the variable speed wind turbines in the presence of uncertainties: a comparison between H∞ and PID controllers. Energy 2015;90:1508–21. https://doi.org/10.1016/j.energy.2015.06.100.
[33] Senjyu T, Sakamoto R, Urasaki N, Higa H, Uezato K, Funabashi T. Output power control of wind turbine generator by pitch angle control using minimum variance control. Electr Eng Jpn 2006;154:1455–63. https://doi.org/10.1002/eej.20247.
[34] Hatami A, Moetakef-imani B. Innovative adaptive pitch control for small wind turbine fatigue load reduction R. Mechatronics 2016;40:137–45. https://doi.org/10.1016/j.mechatronics.2016.10.006.
[35] Abdalrahman G, Melek W, Lien FS. Pitch angle control for a small-scale Darrieus vertical axis wind turbine with straight blades (H-Type VAWT). Renew Energy 2017;114:1353–62. https://doi.org/10.1016/j.renene.2017.07.068.
[36] Li C, Xiao Y, Xu Y, Peng Y, Hu G, Zhu S. Optimization of blade pitch in H-rotor vertical axis wind turbines through computational fluid dynamics simulations. Appl Energy 2018;212:1107–25. https://doi.org/10.1016/j.apenergy.2017.12.035.
[37] Paraschivoiu I, Trifu O, Saeed F. H-Darrieus wind turbine with blade pitch control. Int J Rotating Mach 2009;2009:505343. https://doi.org/10.1155/2009/505343.
[38] Barrett R, Ning A. Comparison of airfoil precomputational analysis methods for optimization of wind turbine blades. IEEE Trans Sustain Energy 2016;7:1081–8. https://doi.org/10.1109/TSTE.2016.2522381.
[39] Templin RJ. Aerodynamic performance theory for the NRC vertical-axis wind turbine. J Energy 1982;6:406–21.
[40] Wilson RE, Lissaman PBS. Applied aerodynamics of wind power machines. Natl Sci Found 1974.
[41] Paraschivoiu I. Aerodynamic loads and performance of the Darrieus rotor. J Energy 1982;6:406–12. https://doi.org/10.2514/3.62621.
[42] Cardona JL. Flow curvature and dynamic stall simulated with an aerodynamic free-vortex model for VAWT. Wind Eng 1984:135–43.
[43] Vallverdu D. VAWT analysis. 2021. https://www.mathworks.com/matlabcentral/fileexchange/46909-vawt-analysis. [Accessed 14 July 2021].